

## Cylinders with Square Cross Section: Paths to Turbulence with Various Angles of Incidence

Matthew J. Fitzgerald<sup>1</sup>, Gregory J. Sheard<sup>1,2</sup> & Kris Ryan<sup>1</sup>

<sup>1</sup> Fluids Laboratory for Aeronautical and Industrial Research (FLAIR), Department of Mechanical Engineering, Monash University, VIC 3800, Australia.

<sup>2</sup> Monash University Biomedical Engineering Technology Alliance (MuBeta), Monash University, VIC 3800, Australia.

### Abstract

The path to turbulence in the wake of cylinders with square cross-section is investigated by means of direct numerical simulation, employing a two-dimensional spectral element method and Floquet linear stability analysis. The critical Reynolds number for the onset of the three-dimensional instability modes A, B, C and QP are reported for cylinder incidence angles between 0° and 45°. The Strouhal—Reynolds number relationship, and lift and drag coefficients are also investigated for these incidence angles. Reynolds numbers (based on the side length of the square) up to  $Re=300$  are considered, and a significant variation in bifurcation scenarios are observed for the various incidence angles.

At Reynolds numbers greater than  $Re \approx 225$  for an incidence angle of 45°, a previously unreported asymmetry is detected in the von Kármán vortex street. The cause of this asymmetry is investigated as it presents a possible alternative path to turbulence to that reported in the wakes of other bluff bodies.

*Keywords:* Instability, wake, square cylinder, incidence angle, Floquet stability analysis, spectral element method

### Introduction

The transition from two-dimensional to three-dimensional flow around a bluff body is an important phenomenon to understand, as the wake forces can have potentially detrimental structural or positional effects on the body or its surrounds. The pressure, lift and drag forces on bodies are altered by three-dimensional flow structures [20]. In the emerging field of micro-technology, flow situations often occur within the Reynolds number range at which the flow transitions to turbulence. The three-dimensional wake structures that develop at the onset of three-dimensional flow have also been observed to persist to Reynolds numbers as high as 10,000 [12]. Understanding the behaviour of the wake at transition can indicate the likely behaviour of the wake at higher Reynolds numbers, without resorting to resolving the turbulent wake.

The transitional behaviour of bluff body wakes has been the subject of numerous numerical and experimental investigations. These studies have examined cylindrical geometries with circular [1, 7, 9, 20, 21, 22] elliptical [17], and square [10, 11, 13, 14, 19] cross sections. Previous results have indicated that the bifurcation scenarios are dependant on the symmetry of the body about the wake centreline. Circular cylinders have been conclusively shown [3] to produce two-dimensional wakes that are unstable to two synchronous three-dimensional modes, labelled modes A and B, as

well as a quasi-periodic mode, labelled mode QP, characterised by a complex pair of Floquet multipliers ( $\mu$ ). Cylinder geometries that are asymmetric about the wake centreline tend to be unstable to a third, subharmonic mode with  $\mu = -1$  (see mode C in the wake of rings [15, 16]) rather than a quasi-periodic mode.

The effect of altering the symmetry of the bluff body, while investigating the stability of the wake to three-dimensional instability modes, was investigated for cylinders with elliptical cross sections [17] and for rings [15, 16], which approach a symmetrical body as the aspect ratio approaches infinity. To the knowledge of the authors, the stability of the square cylinder wake at varying angles of incidence,  $\alpha$ , has not yet been investigated.

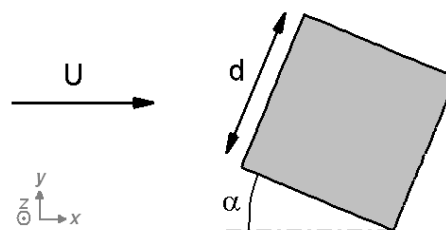


Figure 1 – Schematic representation of the problem under investigation. The coordinate system  $\{x,y,z\}$  is defined at left.

Throughout the current study the Reynolds number (1) is based on the normalised side length of the cylinder,  $d$ , the normalised fluid velocity,  $U$ , and the normalised kinematic viscosity  $\nu$ . Figure 1 schematically illustrates  $U$ ,  $d$  and  $\alpha$ .

$$Re = \frac{Ud}{\nu} \quad (1)$$

The Strouhal number (2) is defined below, where  $f$  is the frequency at which vortices are shed in the wake of the cylinder.

$$St = \frac{fd}{U} \quad (2)$$

The drag coefficient,  $C_D$  and lift coefficient,  $C_L$  scale with the factor  $\frac{1}{2}\rho U^2(1)d$ , and therefore represent coefficients per unit length.

It should be noted that the “traditional” Reynolds number may be determined by multiplying equation (1) by the scale factor:

$$SF = \sin(\alpha) + \cos(\alpha) \quad (3)$$

### Previous Studies

The paths to turbulence over bluff bodies have been investigated for cylinders with square cross section both experimentally [10, 11] and numerically [11, 13, 14, 19]. However, no previous study has investigated the available instability modes for non-zero incidence angles.

The critical Reynolds number for transition to Modes A, B and C were calculated [13] as  $162 \pm 12$ ,  $190 \pm 14$  and  $200 \pm 5$ , respectively. The modes were observed to be most unstable to spanwise perturbations with wavelengths of  $5.22d$ ,  $1.2d$  and  $2.8d$ , respectively. These values are all within the error limits of values specified in other studies. Notably, the critical transition Reynolds numbers for Modes A and B were found experimentally [10] to be approximately 160 and 200 – verifying the results of the numerical studies and the use of linear stability analysis.

The most common technique used to calculate the stability of a bluff body wake to three-dimensional perturbations is the method of Floquet stability analysis. The technique involves measuring the temporal development of an infinitesimally small three-dimensional perturbation, superimposed onto the two-dimensional base-flow. The magnitude of the perturbation is amplified over each shedding cycle by the Floquet multiplier, which when greater than unity, leads to a wake instability. A full description is found in Barkley and Henderson [1]. This method not only significantly reduces the complexity of the simulation over a three-dimensional method, but also clearly elucidates the critical transition Reynolds numbers and spanwise wavelengths.

While Floquet stability analysis reveals the stability of the wake to a particular spanwise perturbation wavelength, the topology of the mode is determined by inspecting the structure of the perturbation field. Mode A has been characterised as having alternating positive and negative streamwise vorticity between successive half periods at a given point along the span [4, 13]. The vorticity also varies periodically in the spanwise direction along the cylinder, with the overall Mode exhibiting a T-periodic temporal symmetry. Mode B is also synchronous with the base flow and is characterised as having constant streamwise vorticity through time, at a given spanwise location. The vorticity also alternates in sign periodically along the span, akin to the Mode A instability. Mode C has been observed in the wakes of rings [15] and the circular cylinder with the presence of a trip-wire [23]. In these cases mode C has been classified as being precisely 2T-periodic (subharmonic). Mode C was not reported in the wake of elliptical cylinders [17].

Blackburn *et al.* [2] explained that the Mode S that was reported in square cylinder wakes [13] is actually a quasi-periodic mode, characterised by a complex pair of Floquet multipliers. The numerical method originally implemented had not allowed a differentiation between complex-conjugate multipliers and a single, real multiplier, as the technique only measured the absolute magnitude of the multipliers. The mode was subsequently renamed mode QP, which was observed to operate via both standing and travelling waves.

Throughout this study, the observed modes will be compared to those from previous studies, in order to identify them and classify

them according to their most unstable spanwise wavelength, and their temporal symmetry. Blackburn *et al.*, [3] explained that when varying only a single parameter,  $Re$ , only one bifurcation can be observed as the primary bifurcation. It was noted that by varying a second parameter such as the body geometry, other bifurcation scenarios were possible.

In the case of quasi-periodic instability modes, the Floquet multiplier magnitude is oscillatory due to the use of a single dimension vector to represent the Floquet multiplier. Blackburn *et al.* [2] explained that when using this method, the values of the Floquet multiplier oscillate about the constant value determined using a Krylov subspace method, which is sufficiently general to compute complex-conjugate pair eigensystems. Therefore when determining the Floquet multiplier values for quasi-periodic modes in this study, the average value of the oscillations will be used as an estimate of the steady Floquet multiplier value, and stability of the system to these perturbation wavelengths.

### Methodology

The present study employs a spectral-element computational fluid dynamics package, which is used to solve the incompressible time-dependant Navier-Stokes equations. Details of the computational method may be found in Karniadakis and Triantafyllou [7]. This method has been used previously to simulate various wake flows [15, 20] and is further validated within this report.

The two-dimensional grid used to discretise the Navier-Stokes equations is shown in Figure 2. The grid is divided into 616 macroelements, each element containing  $N \times N$  interpolation nodes, with are placed to correspond to Gauss-Legendre-Lobatto quadrature points.

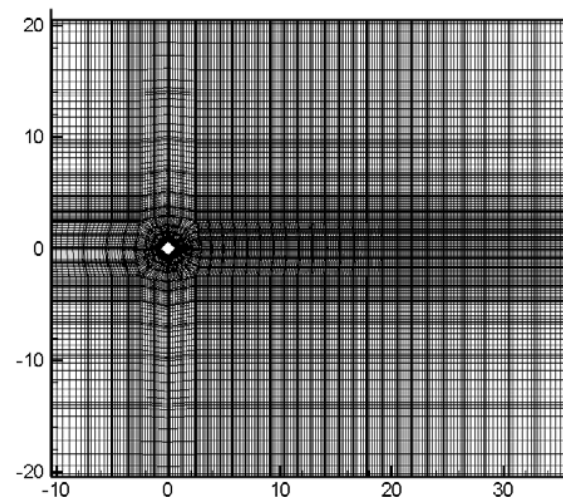


Figure 2 – The computational domain used in this study. The mesh has 616 elements and 81 nodes per element. The blockage ratio varies between 2.5% for the  $0^\circ$  incidence angle and 3.54% for the  $45^\circ$  incidence angle.

In order to determine the most efficient mesh resolution for the present study, a grid resolution study was performed. The number of mesh nodes varies approximately with  $N^2$ , resulting in a non-linear computational expense with increasing resolution. The results of higher-resolution simulations are quite similar once a certain

resolution is used; rendering further resolution increases an inefficient use of computational resources. The Strouhal number has been used previously [17, 20] to determine an appropriate spatial resolution; therefore this method is also used in this study.

The results of the grid resolution study are presented in Figure 3. The discrepancy between the Strouhal numbers of the N=9 and N=11 simulations is ~0.025%, and between N=11 and N=13 simulations is ~0.01%. The small differences involved with using a grid resolution of N=9 to higher resolution grids, led to the conclusion that N=9 was adequate for the current study. The resulting mesh contains 49896 nodes. In comparison, Sohankar *et al.* [19] used a two-dimensional mesh containing 20449 nodes.

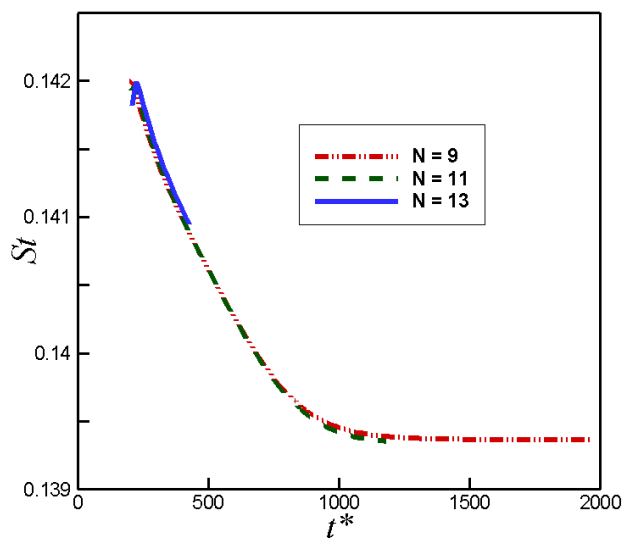


Figure 3 – Results of the grid resolution study, computed at  $Re=100$ ,  $\alpha=45^\circ$ .  $t^*$  is a scaled time allowing for easier comparison of each simulation, as the onset of vortex shedding occurred at slightly different times.

The time step (normalised by  $d/U$ ) used in all simulations in the current study is 0.001. This time step is significantly smaller than that used in previous studies, and was chosen to ensure stability of the simulations. The numerical method used in the present study yields third-order time accuracy.

Sohankar *et al.* [18] reported a reduction in the Strouhal number of 1.4% as the blockage ratio was reduced from 5% to 2.5%. These correspond to the values used in Robichaux *et al.* [13] and the present study respectively. Increasing the upstream and downstream domains past 10d and 26d respectively did not alter results by more than a few percent even for  $\Delta t = 0.025$ . In the current study, an upstream domain of 10d was used, with a downstream domain of 35d, chosen to capture important detail in the far wake.

### Results – Floquet Analysis

A linear stability analysis was performed on three angles of incidence. The cases studied were  $0^\circ$ , in order to compare the results of the present mesh to previous studies;  $45^\circ$ , which is the maximum possible incidence angle; and  $22.5^\circ$ , which is the

midpoint between the two angles. The results of the stability analysis are shown in Figures 4a-c. For the stability analysis, the oscillatory base flow was deemed to have become periodic when the period was constant to 6 significant figures.

Figure 4a shows the results for the  $0^\circ$  incidence angle case. Three simulations were run at Reynolds numbers of 162, 190 and 200, corresponding to the critical transition Reynolds numbers for Modes A, B and QP, as reported by Robichaux *et al.* [13]. Mode A was observed to become critical at  $Re = 162$ , Mode B at  $Re = 193.5 \pm 1$ , and Mode QP at  $Re = 210 \pm 5$  with critical spanwise wavelengths of 5.24d, 1.14d and  $\sim 2.62d$  respectively. Over all Reynolds numbers tested, Mode A was the dominant instability.

In the present study the critical Reynolds numbers differ to those reported in Robichaux *et al.* [13], though the Floquet multiplier magnitude is quite sensitive to  $Re$ . Given the uncertainty associated with the values quoted in Robichaux *et al.* [13], as well as the higher resolution in the current computations, it is likely that the results of the present study are more representative of real flows.

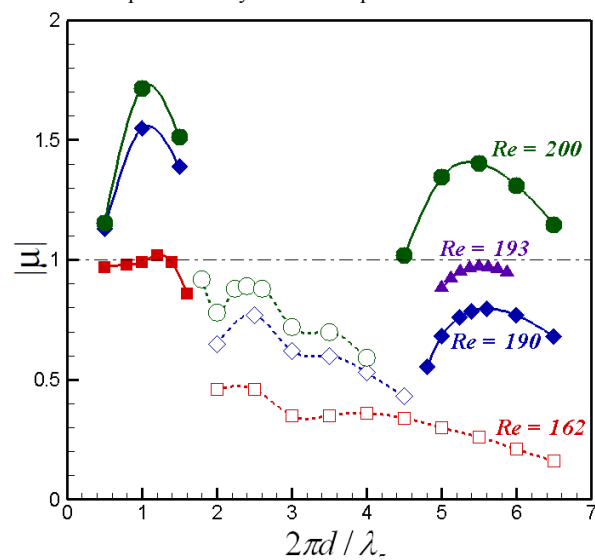


Figure 4a – Results of the Floquet stability analysis at  $0^\circ$ . Filled symbols and solid lines represent real Floquet modes, whereas open symbols and dashed lines represent quasi-periodic modes.  $|\mu|$  is the magnitude of the Floquet multiplier, and  $\lambda_z$  is the spanwise perturbation wavelength. A dash-dotted line represents the neutral stability threshold.

The  $Re = 162$ ,  $\alpha = 0^\circ$  case exhibited oscillating Floquet multipliers at shorter spanwise wavelengths, contrary to previous studies and to higher Reynolds number cases in the present study. The magnitude of oscillation at these wavelengths was minimal and indicates that the mode is either only slightly quasi-periodic in nature, or more likely that the stability analysis had not yet reached a saturated state. For each simulation at this incidence angle, the medium wavelength Floquet multipliers were highly oscillatory, confirming the results of previous studies, which have indicated that the wake is unstable to a quasi-periodic mode over the Reynolds number range under investigation.

The results of the  $\alpha = 22.5^\circ$  case are presented in Figure 4b. The three different simulations each contained two distinct peaks of instability, corresponding to two synchronous instability modes. This cylinder geometry is initially unstable to a shorter wavelength mode with a spanwise wavelength of  $\sim 2.09d$ , at a Reynolds number of  $111 \pm 1$ . At a Reynolds number of 125 the wake became unstable to a second mode, with a spanwise wavelength of  $5.56d$ . The stability analysis revealed a number of quasi-periodic Floquet multipliers, over a narrow range of span-wise perturbation wavelengths.

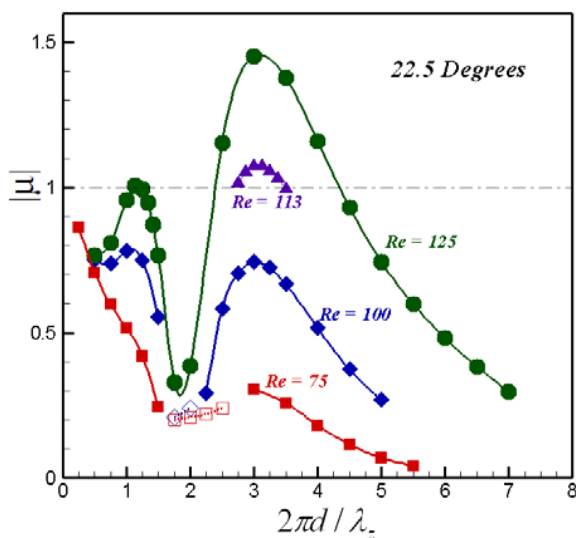


Figure 4b – Results of the Floquet stability analysis at  $22.5^\circ$ . Real and quasi-periodic modes are denoted in the same manner as in Figure 4a.

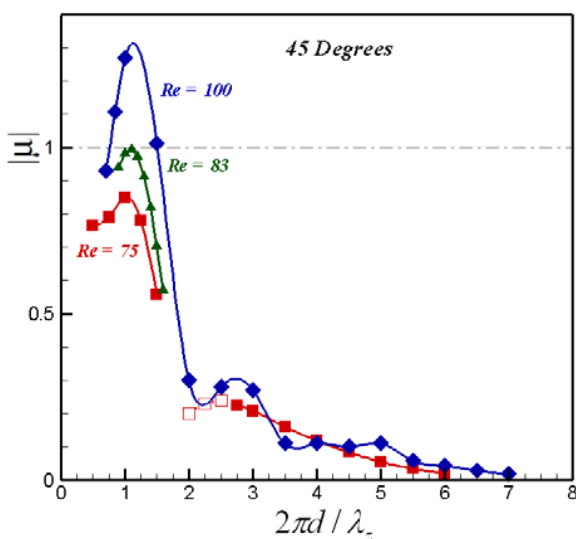


Figure 4c – Results of the Floquet stability analysis at  $45^\circ$ . Real and quasi-periodic modes are denoted in the same manner as in Figure 4a.

Figure 4c shows the results of the Floquet stability analysis for the  $45^\circ$  case. Simulations at higher Reynolds numbers were prevented by an aperiodic two-dimensional base-flow. From the simulations at this incidence angle, an instability mode was resolved, which occurred at a Reynolds number of 83, with a spanwise perturbation wavelength  $5.7d$ . No significant secondary peaks in instability were observed at shorter wavelengths, and in general, shorter wavelength modes were strongly attenuated.

The results show a trend towards suppression of the shorter wavelength modes as the angle of incidence is increased. The critical Reynolds number,  $Re_{cr}$  for each three-dimensional instability was found to decrease with increasing incidence angle. Also, the proportion of wavelengths for which quasi-periodic modes are available generally diminishes with increasing incidence angle, and for higher Reynolds numbers. Sheard *et al.* [17] also reported a decrease in  $Re_{cr}$  and the proportion of quasi-periodic modes, with increasing  $\alpha$ , for elliptical cylinders. These trends could be investigated further with intermediate incidence angles, to confirm the consistency of the observations.

#### Results – Mode Characteristics

At each of the peaks for Figures 4a-c, streamwise vorticity plots were produced in order to reveal the spatiotemporal symmetry of each instability mode. These are shown for the  $0^\circ$  incidence angle case in Figures 5a-c.

The vorticity plots in Figures 5a-c show contours that are comparable to those of Robichaux *et al.* [13]. In both studies Mode A is observed to have alternating streamwise vorticity every half-cycle, mode B has constant streamwise vorticity with time, and Mode QP (or “Mode S”) exhibits approximately  $2T$  spatiotemporal symmetry.

Figures 6a-c show the streamwise vorticity for the two instability peaks in Figure 4b. In Figure 6a, the first peak is revealed to have topology equal to that of Mode A for the  $0^\circ$  case, and the spanwise wavelength of  $5.24d$  corresponds closely to previously reported values for Mode A in the wake of cylinders with square cross section [13].

Figures 6b and c show a subharmonic Floquet mode – the vorticity contours were observed to alternate between Figures 6b and c over time. After starting transients had decayed, the Floquet multipliers for this instability peak reached a constant value, indicating that the mode is not quasi-periodic, while the vorticity contours highlight the  $2T$  periodic, subharmonic nature of the mode. Mode C was predicted to have wavelengths of  $2d$  and  $1.7d$  in the wakes of circular cylinders [23] and rings [15] respectively. The present value of  $2.09d$  agrees closely with the value for circular cylinders.

The streamwise vorticity of the most unstable Floquet mode in the  $45^\circ$  case is shown in Figure 7. As with the other two cases, this mode displays a spatiotemporal symmetry consistent with Mode A observed in the wake of other bluff bodies. The spanwise wavelength for the most unstable Floquet multiplier in this case is  $\sim 6d$ , which is similar to reported values for Mode A in other studies.

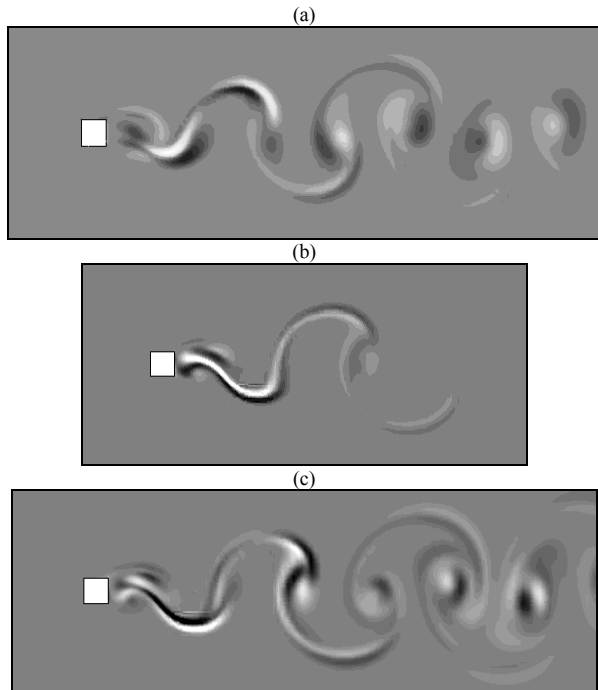


Figure 5 – Plots of streamwise vorticity  $\omega_z$  for the  $0^\circ$  incidence angle case.

Arbitrary contour levels are chosen to reveal the structure of the perturbation field. (a) Mode A,  $Re_{cr} = 162$   $\lambda_{cr} = 5.24d$  (b) Mode B,  $Re_{cr} = 193.5 \pm 1$   $\lambda_{cr} = 1.14d$  (c) Mode QP,  $Re_{cr} = 210 \pm 5$   $\lambda_{cr} = 2.62d$ .

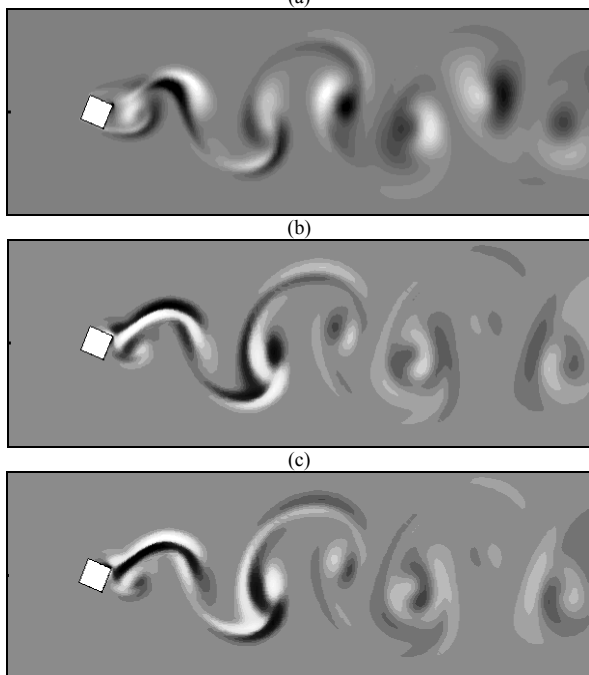


Figure 6 – Plots of streamwise vorticity  $\omega_z$  for the  $22.5^\circ$  incidence angle case. Arbitrary contours are chosen as in Figure 5. (a) Mode A,  $Re_{cr} = 125$   $\lambda_{cr} = 5.56d$  (b,c) Mode C,  $Re_{cr} = 111 \pm 1$   $\lambda_{cr} = 2.09d$ . (Images b and c are separated by 1 shedding period,  $T$ .)



Figure 7 – Plot of streamwise vorticity  $\omega_z$  for the  $45^\circ$  incidence angle case, showing Mode A,  $Re_{cr} = 83$   $\lambda_{cr} = 5.7d$ . Arbitrary contours are chosen as in Figure 5.

### Results – Asymmetric Wake

At Reynolds numbers of 200 and above, an asymmetry was observed in the wake of the  $45^\circ$  cylinder. This asymmetry was observed consistently for grids of resolution  $N=5$  to  $N=11$ , demonstrating that the phenomenon was not an artefact of grid resolution. After travelling downstream from the cylinder, the von Kármán vortices were observed to travel away from the wake centreline at an angle, as shown in Figure 8. Sohankar *et al.* [19] mentioned this effect briefly for their two-dimensional simulations around square cylinders at  $0^\circ$  incidence angle. As their study focussed on three-dimensional simulations, they did not investigate this phenomenon in any detail. As with the present study, the asymmetry in the wake resulted in an average net lift coefficient. For the present study, at  $Re=225$ , this net lift coefficient was measured at  $C_L \approx -0.20$ .

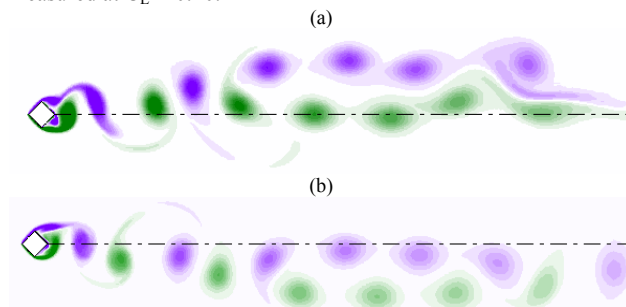


Figure 8 – Plots of spanwise vorticity, highlighting asymmetry in the wake for two different simulations.  $Re = 225$ ,  $\alpha = 45^\circ$  (a)  $N = 9$  (b)  $N = 11$ .

The asymmetry in the wake became more pronounced at higher Reynolds numbers, which is highlighted qualitatively in Figure 9. The direction of vortical propagation remained biased to one side of the wake region, for at least 50 shedding cycles. It is likely that the mechanism responsible for this asymmetric von Kármán vortex street is self-propagating, and the direction of propagation is determined by the initial perturbations that initiate the vortex street.

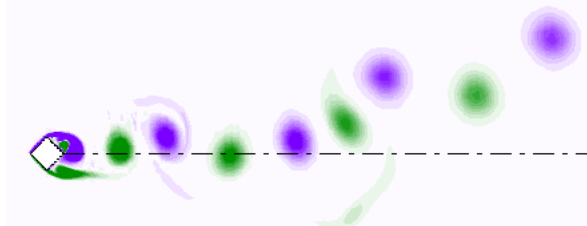


Figure 9 – Asymmetric wake at  $Re = 350$ ,  $\alpha = 45^\circ$ ,  $N=7$ .

In order to investigate the origin of this asymmetry, simulations at  $Re = 225, 250$  and  $275$  were performed using a  $45^\circ$  cylinder with a rounded (circular) downstream corner. The profile of this cylinder is shown in Figure 10. Using the new cylinder profile, the vortices travelled downstream in a symmetric manner, and no net lift coefficient was measured. This indicates that the asymmetry is due to the sharp corner at the rear of the standard  $45^\circ$  cylinder. It is likely that the corner serves to develop a pressure differential between the upper and lower sides of the rear of the cylinder, which affects the direction at which each vortex is shed. Rounding the cylinder smooths the pressure gradient and allows any initial asymmetries to dampen out until a steady, symmetric state is achieved, as is observed in circular cylinder wakes.

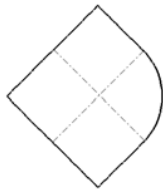


Figure 10 – Schematic of the rounded  $45^\circ$  cylinder.

It should be pointed out that this two-dimensional asymmetry occurs at Reynolds numbers higher than those observed for the transition to three-dimensional flow. Therefore it is not possible to determine if the three-dimensional structure in the wake will suppress this asymmetry, or whether the three dimensional structure will instead be affected by the asymmetry. A full three-dimensional simulation or experimental method would be required to determine the true transitional nature of the wake for the  $45^\circ$  cylinder.

### Results – Wake-Splitting

The cylinder wakes were observed to split into two distinct vortex streams, before recombining again further downstream. This was observed over all Reynolds numbers tested, from  $Re=50$  to  $Re=300$ . As the vortex pairs re-combined downstream, merging of co-rotating vortices was observed, which lead to an increasingly unsteady wake as the Reynolds number was increased. Due to the extent of the downstream domain, the chaotic recombination region was only observed for Reynolds numbers greater than 150, as the vortices combined further downstream for lower Reynolds numbers. The splitting region gradually travelled upstream over time, which significantly increased the time required for the wake to reach a saturated state. This is shown in Figure 11a and 11b.

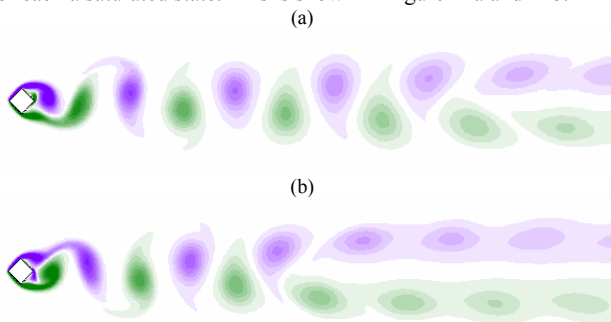


Figure 11 – Vorticity contours at (a)  $t = 232$  and (b)  $t = 562.5$  ( $\alpha = 45^\circ, Re = 100$ ).

The wake-splitting phenomenon was reported and investigated both numerically and experimentally [5,6] in the wakes of circular cylinders. These studies reported the emergence of a secondary vortex street in the far wake, which developed after the merging of the primary vortex street. It is possible that this secondary street also forms in square cylinder wakes, however as the primary objectives of this study do not concern this phenomenon, it is not investigated any further.

### Results – $St, C_D, C_L$ dependence on $Re, \alpha$

The results of this section are for two-dimensional numerical simulations. It should be noted that they span a Reynolds number range that exceeds the critical Reynolds numbers for three-dimensional instability. As this study does not use a three-dimensional grid, the results may differ from past or future experimental values due to these three-dimensional interactions.

The Strouhal number was determined in each simulation by monitoring the velocity in the  $y$ -direction over time, at a point  $3d$  downstream from the centre of the cylinder, and in the wake centre-line. This point was chosen because it was located on the vertex of a mesh element and consequently remained fixed for alternate grid resolutions. The determination of the Strouhal number was not only required for the Floquet stability analysis, but also provides an avenue for verifying the current computational method.

The Strouhal number variation with Reynolds number is plotted in Figure 12 for the three different incidence angles. The results for the  $0^\circ$  cylinder are qualitatively similar to those of Robichaux *et al.* [13] however the numerical values differ by up to 10%. Previous studies [18] have shown that increasing the blockage ratio leads to an increase in  $St$ , which could explain the discrepancy in the Strouhal numbers. To verify this, the results of a high blockage mesh are shown in Figure 12. The results of Robichaux *et al.* [13] were within 2% of the values produced by Franke *et al.* [4], who used a 1<sup>st</sup> order time-accurate numerical method, a time step of  $\Delta t = 0.025$ , and a blockage ratio of 8.3%, which is larger than the blockage ratio of 2.5% in the present study. Blockage and time step effects account for the 10% discrepancy and highlight the accuracy of the present numerical method.

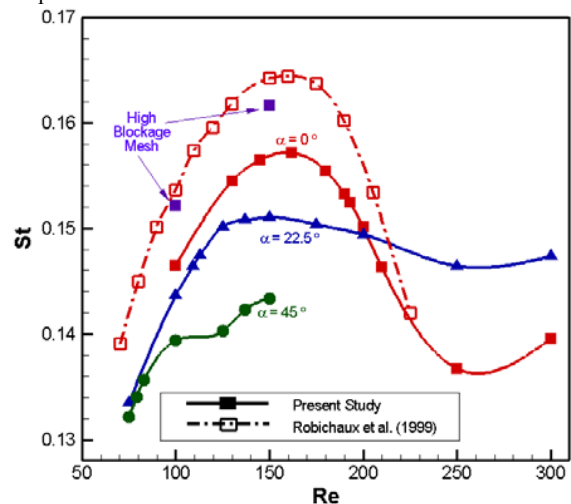


Figure 12 –  $St-Re$  plots for the three incidence angles.

A peak in the Strouhal number was observed in the 0° cylinder at  $Re \approx 162$ , with a local minimum at  $Re \approx 210$ . This peak was observed in previous studies, however for circular cylinders,  $St$  increases continuously with  $Re$  [8]. As the incidence angle was increased, the peak became less pronounced, and the maximum Strouhal number was reduced. At Reynolds numbers above those shown in Figure 12, the wake was too chaotic to determine the Strouhal number.

The average drag coefficient  $\overline{C_D}$  is shown in Figure 13. The figure shows a clear increase in the average drag coefficient as the incidence angle is increased. The drag dependence on the Reynolds number was minimal for lower incidence angles, with the incidence angle exerting a much stronger influence on drag.

The drag coefficient in equation (2) scales with the cylinder side length, rather than the projected height of the cylinder. If this scaled height is used, the drag coefficients become more closely grouped, however there is still some discrepancy. This is due to the separating and recirculating flow behind the body, which causes an “effective” height that is greater than just the body itself - a phenomenon that was discussed by Robichaux *et al.* [13]. The blockage ratio also increases with increasing incidence angle, from ~2.5% to ~5%, which may alter the drag coefficient. Rounding the back of the 45° cylinder reduced the average drag coefficient by approximately 30%, to ~2, due to less inhibited vortex shedding.

Figure 14 shows the average lift coefficient  $\overline{C_L}$  variation with Reynolds number for the three cases. As expected, the symmetrical 0° and 45° cases experienced virtually no net lift for lower Reynolds numbers. The asymmetric 22.5° cylinder experienced an almost negligible positive lift coefficient at low Reynolds numbers, which became negative at  $Re=125$ , and increased in magnitude as the Reynolds number was further increased.

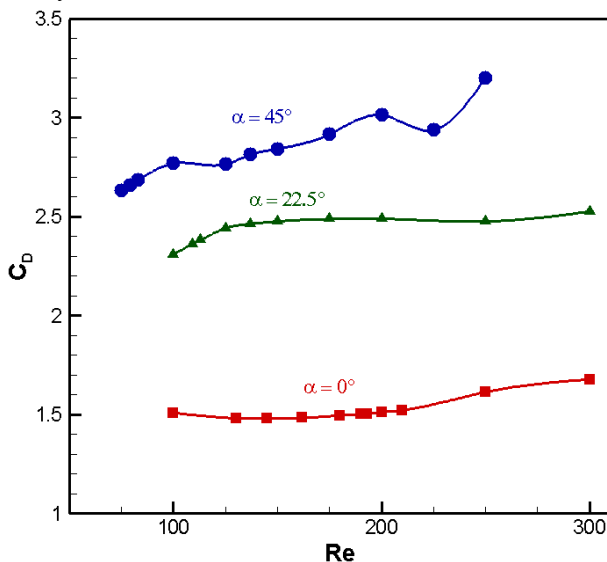


Figure 13 – Average drag coefficients for the three cases.

The direction of the net lift force changed direction due to the variation of the viscous and pressure forces. At lower Reynolds

numbers the viscous forces were slightly greater in magnitude, while the pressure forces were responsible for the net negative lift coefficient at higher Reynolds numbers. The net lift force for the cylinder at  $\alpha = 45^\circ$ , at higher Reynolds numbers, was entirely due to pressure forces. These were a consequence of the asymmetric vortex shedding. The direction in which the asymmetry operates is arbitrary, so the absolute magnitude of the lift coefficient is more important than the sign in this case.

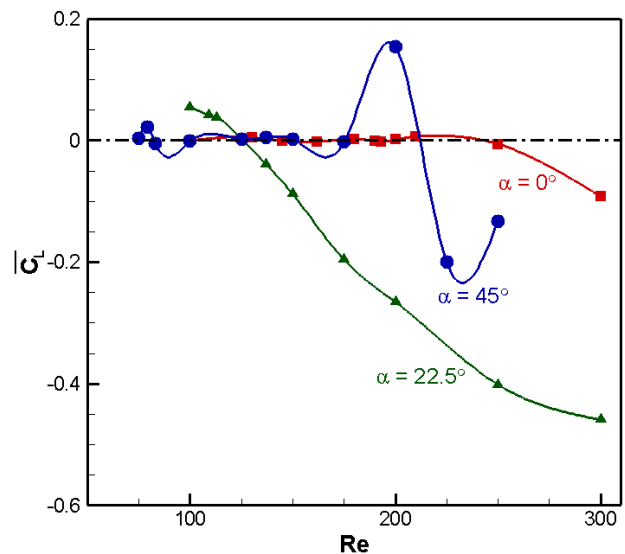


Figure 14 – Average lift coefficients for the three cases.

**Conclusions**

The three-dimensional transition scenarios in the wake of a square cylinder were determined for angles of incidence 0°, 22.5° and 45°. Critical transition Reynolds numbers  $Re_{cr}$  and spanwise perturbation wavelengths  $\lambda_{cr}$  were found for each instability mode and are listed in Table 1. As predicted previously [3], via altering  $Re$  and a second parameter  $\alpha$ , alternative bifurcation scenarios were observed. Also consistent with previous results [2] was the observation that only bluff body geometries that are asymmetric about the wake centreline are unstable to subharmonic modes.

The stability analysis revealed that Mode A operates in the wake of all three cylinder geometries, as shown by the lower hatched line in Figure 15. Also shown in Figure 15 is a second hatched line, which marks an approximate transition zone where the wake becomes unsteady to the point where Floquet stability analysis is no longer possible. The results of the 0° cylinder supported the findings of Robichaux *et al* [13], with the exception that mode “S” was quasi-periodic as predicted by Blackburn and Lopez [2]. With increasing incidence angle, shorter wavelength modes, as well as quasi-periodic modes, became less prevalent.

$\alpha$	0°			22.5°		45°
<b>Mode</b>	A	B	QP	C	A	A
<b>Re<sub>cr</sub></b>	162	193.5±1	210±5	111±1	125	83
<b>λ<sub>cr</sub></b>	5.24d	1.14d	2.62d	2.09d	5.56d	5.7d

Table 1 – Summary of numerical results of the Floquet stability analysis.

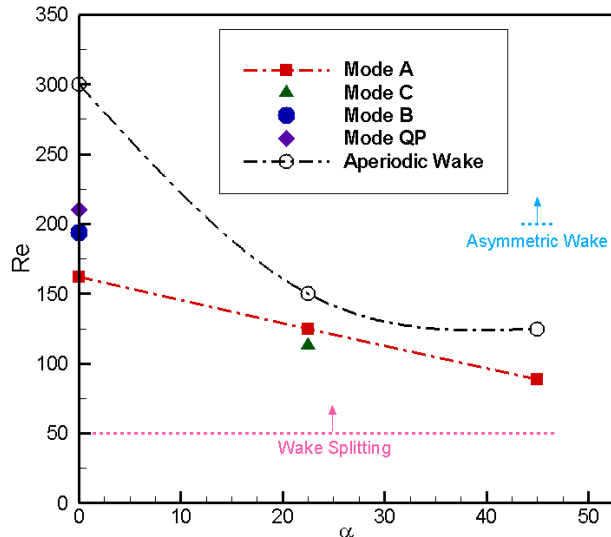


Figure 15 – Summary of results of the parameter space under investigation.

The square cylinder wakes exhibited a spitting and recombination phenomenon over all  $Re$  tested (50 and above). For  $Re=200$  and above, the  $45^\circ$  cylinder wake became asymmetric, which resulted in a net lift coefficient of order  $\|C_L\| = 0.2$ .

The Strouhal number reached a peak of 0.157 at a  $Re=160$ , for the  $0^\circ$  cylinder. At other incidence angles, the peak in the  $Re$ - $St$  curve was less prominent. In general, the Strouhal number decreased with increasing incidence angle. The average drag coefficient was amplified as the incidence angle was increased, due to a larger deflection of the incident flow. The Reynolds number did not have a significant impact on the average drag coefficient. The symmetric bluff body geometries experienced negligible average lift forces at low Reynolds numbers. As mentioned, for the  $45^\circ$  cylinder, a lift force was observed at Reynolds numbers of 200 and above, due to asymmetric vortex shedding. The  $22.5^\circ$  cylinder experienced a lift force for all Reynolds numbers, due to its asymmetric profile and consequential unbalanced fluid deflection.

#### Acknowledgements

The computational resources of the Australian Partnership for Advanced Computing were utilized to complete this study, thanks to a time allocation under the Merit Allocation Scheme.

#### References

[1] Barkley, D. and Henderson, R. D., 1996. Three-dimensional Floquet stability analysis of the wake of a circular cylinder. *Journal of Fluid Mechanics*, **322**, 215-241.  
 [2] Blackburn, H. M. and Lopez, J. M., 2003. On three-dimensional quasiperiodic Floquet instabilities of two-dimensional bluff body wakes. *Physics of Fluids*, **15**, n 8, L57-L60.  
 [3] Blackburn, H. M., Marques, F. and Lopez, J. M., 2005. Symmetry breaking of two-dimensional time-periodic wakes. *Journal of Fluid Mechanics*, **522**, 395-411.  
 [4] Franke, R. Rodi, W. and Schönung, B., 1990. Numerical calculation of laminar vortex-shedding flow past cylinders. *J. Wind Eng. Ind. Aero.* **35**, 237-257.

[5] Inoue, O. and Yamazaki, T., 1999. Secondary vortex streets in two-dimensional cylinder wakes. *Fluid Dynamics Research*, **25**, 1.  
 [6] Karasudani, T. and Funakoshi, M., 1994. Evolution of a vortex street in the far wake of a circular cylinder. *Fluid Dynamics Research*, **14**, 331-352.  
 [7] Karniadakis, G. E. and Triantafyllou, G. S., 1992. Three-dimensional dynamics and transition to turbulence in the wake of bluff objects. *Journal of Fluid Mechanics*, **238**, 1-30.  
 [8] Noack, B. R. König, M. and Eckelmann, H., 1993. Three-dimensional stability analysis of the periodic flow around a circular cylinder. *Phys. Fluids A* **5**, 1279.  
 [9] Leweke, T. and Williamson, C. H. K., 1998. Three-dimensional instabilities in wake transition. *European Journal of Mechanics – B/Fluids*, **17**, n 4, 571-586.  
 [10] Luo S. C., Chew Y. T. and Ng. Y. T., 2003. Characteristics of square cylinder wake transition flows. *Physics of Fluids*, **15**, n 9, 2549-2559.  
 [11] Luo, S. C., Tong, X. H. and Khoo, B. C., 2007. Transition phenomena in the wake of a square cylinder. *Journal of Fluids and Structures*, **23**, 227-248.  
 [12] Mansy, H., Pan-Mei Yang and Williams, D. R., 1994. Quantitative measurements of three-dimensional structures in the wake of a circular cylinder. *Journal of Fluid Mechanics*, **270**, 277.  
 [13] Robichaux, J., Balachandar, S. and Vanka S.P. 1997. Three-dimensional Floquet instability of the wake of the square cylinder. *Physics of Fluids*, **11**, 560-578.  
 [14] Saha, A. K., Biswas, G. and Muralidhar, K., 2003. Three-dimensional study of flow past a square cylinder at low Reynolds numbers. *International Journal of Heat and Fluid Flow*, **24**, 54-66.  
 [15] Sheard, G. J., Thompson, M. C. and Hourigan, K., 2003. From spheres to circular cylinders: The stability and flow structures of bluff ring wakes. *J. Fluid Mech.*, 492:147-180.  
 [16] Sheard, G. J. Thompson, M. C. Hourigan, K. and Leweke, T., 2005. The evolution of a subharmonic mode in a vortex street. *J. Fluid Mech.*, 534:23-38.  
 [17] Sheard, G.J., Cylinders with Elliptical Cross-Section: Wake Stability with Incidence Angle Variation, *Proceedings of the IUTAM Symposium on Unsteady Separated Flows and Their Control*, Hotel Corfu Chandris, Corfu, Greece, 18-22 June 2007.  
 [18] Sohankar, A., Norberg, C. and Davidson, L. 1998. Low Reynolds-Number Flow around a square cylinder at incidence: Study of Blockage, Onset of Vortex Shedding and Outlet Boundary Condition. *International Journal for Numerical Methods in Fluids*, **26**, n 1, 39.  
 [19] Sohankar, A., Norberg, C. and Davidson, L. 1999. Simulation of three dimensional flow around a square cylinder at moderate Reynolds numbers. *Physics of Fluids*, **11**, 288-306.  
 [20] Thompson, M. C., Hourigan, K. and Sheridan, J., 1996. Three-dimensional instabilities in the wake of a circular cylinder. *Experimental and Thermal Fluid Science*, **12**, 190-196.  
 [21] Thompson, M. C., Leweke, T., and Williamson, C. H. K., 2001. The physical mechanism of transition in bluff body wakes. *Journal of Fluid and Structures*, **15**, 607-616.  
 [22] Williamson, C. H. K., 1996. Three-dimensional wake transition. *Journal of Fluid Mechanics*, **328**, 345-407.  
 [23] Zhang, H. Q., Fey, U., Noack, B. R., König, M., and Eckelmann, H., 1995. On the transition of the cylinder wake. *Physics of Fluids*, **7**, n 4, 779-794.